

Field driven magnetostructural transitions in GeCo_2O_4

X. Fabrèges,^{1,2} E. Ressouche,³ F. Duc,² S. de Brion,^{4,5} M. Amara,^{4,5} C. Detlefs,⁶ L. Paolasini,⁶ E. Suard,⁷ L.-P. Regnault,³ B. Canals,⁴ P. Strobel,^{4,5} and V. Simonet^{4,5,*}

¹Laboratoire Léon Brillouin, CEA / CNRS, Saclay, France

²Laboratoire National des Champs Magnétiques Intenses, CNRS-INSU-UJF-UPS, 31400 Toulouse, France

³CEA/Grenoble, INAC/SPSMS-MDN, 17 rue des Martyrs, 38054 Grenoble Cedex 9, France

⁴CNRS, Institut Néel, 38042 Grenoble, France

⁵Univ. Grenoble Alpes, Institut Néel, 38042 Grenoble, France

⁶European Synchrotron Radiation Facility, Grenoble, France

⁷Institut Laue Langevin, BP 156, 38042 Grenoble Cedex 9, France

(Dated: September 29, 2016)

In the spinel compound GeCo_2O_4 , the Co^{2+} pyrochlore sublattice presents remarkable magnetic field-induced behaviors that we unveil through neutron and X-ray single-crystal diffraction. The Néel ordered magnetic phase is entered through a structural lowering of the cubic symmetry. In this phase, when a magnetic field is applied along a 2-fold cubic direction, a spin-flop transition of one fourth of the magnetic moments releases the magnetic frustration and triggers magnetostructural effects. At high field, these ultimately lead to an unusual spin reorientation associated to structural changes.

PACS numbers: 75.25.-j, 75.50.Ee, 75.30.Gw, 75.80.+q

I. INTRODUCTION

Spinel compounds with the generic formula AB_2O_4 crystallize in the cubic space group $Fd\bar{3}m$. The B sites can accommodate a magnetic ion, in this case Co^{2+} . They form a pyrochlore lattice, a network of corner-sharing tetrahedra, that is the archetype of geometrical frustration. In addition, they combine magnetic and lattice degrees of freedom, which confer them a magnetostructural flexibility in zero and finite magnetic field. The interplay between magnetic frustration and magnetoelastic coupling has been intensively studied in spinels with, for instance, either V^{3+} or Cr^{3+} on the B site and various ions on the A site (Hg, Mg, Cd and Zn) [1–6]. In these systems, at the Néel temperature (T_N), a transition to an antiferromagnetic (AFM) ordering is accompanied by a cubic to tetragonal or orthorhombic structural distortion. It is interpreted as a 3-dimensional spin-Peierls transition acting to reduce the frustration [1, 3]. In the Cr compounds, when applying a magnetic field, a magnetization plateau at half of the saturation magnetization is stabilized by the spin-lattice coupling on a wide range of fields [2, 3, 7, 8]. Moreover, the beginning of the plateau coincides with a structural distortion. It corresponds to a recovery of the cubic structure as a consequence of the release of the frustration by the magnetic field [4, 5].

Ge spinels, with Ni^{2+} or Co^{2+} on the pyrochlore lattice, have comparable rich phase diagrams but have been less studied because the frustration effects are not as straightforward, in particular not solely driven by the first neighbor interactions. They were both shown, by powder neutron diffraction, to order in a magnetic struc-

ture characterized by a propagation vector $k=(1/2, 1/2, 1/2)$ stabilized through competing interactions beyond the third neighbors [6, 7]. The magnetic arrangement was described assuming a single propagation vector (single- k structure) as follows: alternating kagome (KGM) and triangular (TRI) ferromagnetic (FM) planes, perpendicular to the $\langle 111 \rangle$ directions associated with the propagation vector, and antiferromagnetically coupled to the nearest planes of the same kind (see figure 1a). In GeNi_2O_4 , which retains the cubic structure in the magnetic phase, both KGM and TRI sites are magnetically decoupled, i.e. the molecular field created by the magnetization of one type of site on the other one is zero. It leads to an independent ordering of the two kinds of planes with distinct transition temperatures [11–13]. This is at variance with GeCo_2O_4 in which a unique magnetic transition is observed at $T_N=23.5$ K. This would be due to a structural distortion, proposed to be cubic-to-tetragonal from powder neutron and X-ray diffraction, which couples the two sites and allows to reduce the frustration in the absence of any external magnetic field [4, 15].

Besides this zero-field magnetostructural behavior, a complex H-T phase diagram has been observed in GeCo_2O_4 by magnetization, ultrasound and electron spin resonance measurements, evidencing several field-induced anomalies [4, 7, 12, 16–21]. Their microscopic origin was investigated by powder neutron diffraction under magnetic field up to 10 T [6]. A transition, observed at ≈ 4 T, was attributed to an antiferromagnetic-to-ferromagnetic spin rearrangement between the triangular planes while retaining the antiferromagnetic arrangement between the kagome planes. The final ferromagnetic order of the kagome planes was proposed to occur at the second transition around $H=10$ T.

We hereafter present the results of single-crystal neutron and synchrotron X-ray diffraction under zero and

*Corresponding author: virginie.simonet@neel.cnrs.fr

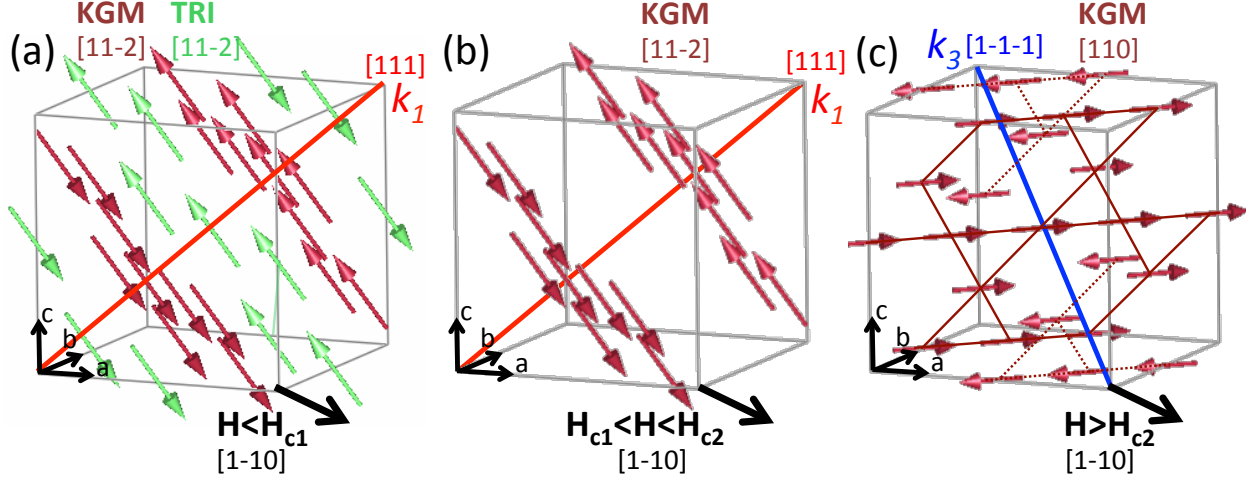


FIG. 1: (a) AFM ordered components of the KGM (red) and TRI (green) moments determined from single-crystal neutron diffraction refinements at 4.5 K and at $H=0$ T for the \mathbf{k}_1 domain (b), at $H=5.5$ T for the \mathbf{k}_1 domain (c) and at $H=12$ T for the \mathbf{k}_3 domain (d). The direction of the propagation vector and of the applied magnetic field are shown.

finite magnetic fields applied along a 2-fold axis of the high temperature cubic structure. We show in particular that the high field transition, for this orientation of the field, is much more subtle than a plain antiferromagnetic-to-ferromagnet one. It implies a change of the magnetic anisotropy, a switch of the magnetostructural domains, and the stabilization of a new canted magnetic structure. We discuss the interplay between magnetostructural effects and frustration in triggering these field-induced unconventional behaviors.

II. RESULTS

Single-crystals of GeCo_2O_4 with an octahedral shape of approximately 2 mm size were synthesized by chemical vapor transport. Neutron diffraction was carried out at the Institut Laue Langevin (ILL), in zero field on the CEA-CRG D15 diffractometer and under magnetic field up to 12 T, applied along the $[1-10]$ direction of the cube, on the CEA-CRG D23 diffractometer. An additional diffraction experiment using polarized neutrons and spherical polarization analysis was performed with the single-crystal installed inside the CRYOPAD device on the CEA-CRG IN22 spectrometer at the ILL. High magnetic field X-ray single-crystal diffraction experiments using synchrotron radiation were performed at the ID06 beamline (ESRF) under magnetic field up to 10 T [23]. Magnetization measurements on an oriented single-crystal were performed using an extraction magnetometer.

A. Magnetic structure in zero and finite magnetic fields

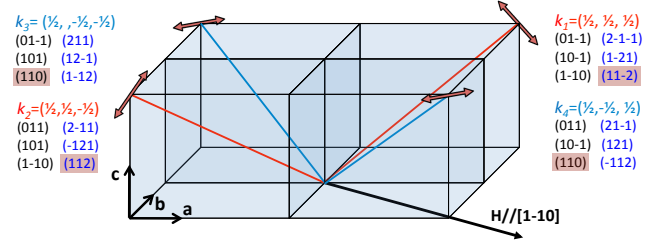


FIG. 2: Magnetic domains in cubic symmetry: direction of the propagation vectors, two of them (red lines) selected between \mathbf{H}_{dom} and \mathbf{H}_{c2} , the other two (blue lines) selected above \mathbf{H}_{c2} . For each k -domain, the 3 S -domains are listed for the magnetic moments either along the $\langle 110 \rangle$ (in black) or along the $\langle 112 \rangle$ (in blue) directions. The red boxes and arrows gives the orientation of the AFM component on the KGM sites for $\mathbf{H}_{\text{dom}} < H < \mathbf{H}_{c2}$ and $H > \mathbf{H}_{c2}$.

To analyze the single-crystal neutron diffraction results of GeCo_2O_4 , we first assume a cubic structure and a simple- k magnetic arrangement. Both hypotheses will be discussed later on. We take into account the presence of several magnetic domains, that appear at the phase transition (see figure 2): we considered four k -domains that correspond to the symmetry-equivalent directions of propagation of the AFM order given by the propagation vectors $\mathbf{k}_1=(1/2, 1/2, 1/2)$, $\mathbf{k}_2=(1/2, 1/2, -1/2)$, $\mathbf{k}_3=(1/2, -1/2, -1/2)$, $\mathbf{k}_4=(1/2, -1/2, 1/2)$. Moreover, if the magnetic moments lie in the $\{111\}$ planes, there are three S -domains per k -domain with moment directions

rotated by 120° between S -domains [24]. In zero field, our refinement of the magnetic intensities collected on D15 [23] confirms the magnetic structure deduced from powder neutron diffraction [6, 7]. It additionally proves that the TRI and KGM magnetic moments lie in the plane perpendicular to the $\langle 111 \rangle$ directions given by the propagation vectors. Due to the presence of 12 domains that we found approximately equipopulated, the moment orientation could not be further determined using unpolarized neutrons. Polarized neutrons and spherical polarization analysis allowed us to determine the relative orientation of the magnetic moments on the TRI and KGM sites (but not their absolute direction that was only inferred from neutron scattering under magnetic field, as presented below). The best fit of the measured polarization matrix for 23 reflections is obtained for parallel TRI and KGM magnetic moments, as shown in figure 1a [23].

Under a magnetic field, the populations of the magnetic domains are expected to vary, the domains with the AFM component perpendicular to the magnetic field being favored by the exchange and Zeeman terms. We followed four reflections while applying a magnetic field along the 2-fold axis $[1-10]$ direction: $(0.5, 0.5, 0.5)$, $(0.5, 0.5, -0.5)$, $(0.5, -0.5, -0.5)$, $(0.5, -0.5, 0.5)$. They are characteristic of the four k -domain populations and have roughly the same intensity at $H=0$. As shown in figure 3a, when increasing the magnetic field, the 4 equipopulated k -domains start to split into two pairs of reflections with different intensities, one pair being selected ($\mathbf{k}_1, \mathbf{k}_2$) whereas the other pair ($\mathbf{k}_3, \mathbf{k}_4$) is suppressed with increasing field. This selection occurs irreversibly mostly below $H_{\text{dom}} \approx 2$ T. At $H_{\text{c1}}=4.3$ T, there is a slight change of curvature of the field dependence of the $(0.5, 0.5, 0.5)$ and $(0.5, 0.5, -0.5)$ signal. This field corresponds to the first anomaly observed in the magnetization curve shown in figure 4, in agreement with the results of Hoshi *et al.* [4]. The second magnetization anomaly occurs at $H_{\text{c2}}=9.5$ T, when the populations of the four k -domains change again abruptly in a remarkable way: the two selected domains ($\mathbf{k}_1, \mathbf{k}_2$) vanish and the two k -domains that were absent ($\mathbf{k}_3, \mathbf{k}_4$) are populated (see figure 3a).

In addition to the AFM components probed with the previous reflections, a gradual rise of the intensity of the $(1, 1, 1)$ nuclear reflection is observed (see figure 3b). It is associated with the FM components M developing along the field on the TRI and KGM sites and leading to the integrated magnetic intensity on the $(1, 1, 1)$ reflection $\propto (M_{\text{TRI}} - 3M_{\text{KGM}})^2$. Two step-like increases of this signal are observed, a small one at H_{c1} and a pronounced one at H_{c2} . Above H_{c2} , both a FM and an AFM contributions are thus present indicating a canted magnetic structure, consistent with the magnetization still increasing in higher fields [7].

The field-induced magnetic orders could be determined from refinements of the magnetic reflections collected on D23 under the selected fields of 5.5, 9.4 and 12 T [23]. The field-induced magnetic behavior is summarized in table I. At $H=5.5$ and 9.4 T, i.e. for $H_{\text{c1}} < H < H_{\text{c2}}$, the

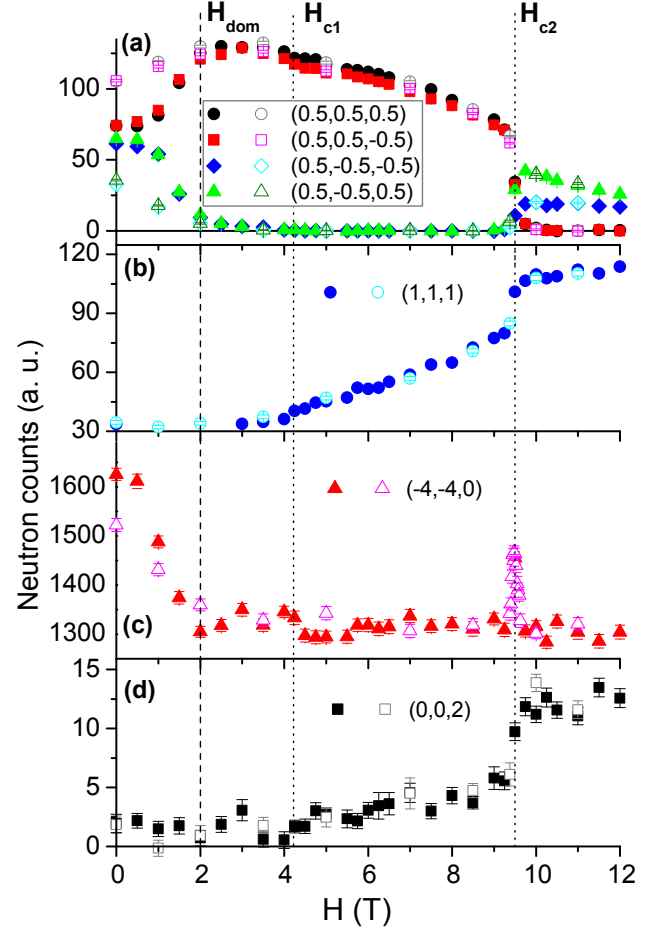


FIG. 3: Neutron counts at the peak maximum versus magnetic field applied along the $[1-10]$ direction at 4.5 K for: (a) 4 magnetic Bragg reflections representative of the k -domains, (b) the $(1, 1, 1)$ weak nuclear reflection on top of which grows a field-induced FM component, (c) the $(-4, -4, 0)$ strong nuclear reflection sensitive to the extinction, (d) the $(0, 0, 2)$ forbidden nuclear reflection. The H_{dom} , H_{c1} and H_{c2} characteristic fields are indicated by vertical lines. The filled (open) symbols correspond to increasing (decreasing) field measurements.

KGM AFM component of the moments is found aligned along the $[11-2]$ direction for the \mathbf{k}_1 selected domain (see figure 1b) and along the $[112]$ direction for the \mathbf{k}_2 selected domain. The amplitude of this component decreases from 3.1 to $1.8 \mu_B$ between 5.5 and 9.4 T while the FM component increases. On the TRI site, the AFM component is found equal to zero above H_{c1} , as already proposed [6]. At $H=12$ T, i.e. for $H > H_{\text{c2}}$, the KGM AFM component of the two new \mathbf{k}_3 and \mathbf{k}_4 selected domains is found aligned along a unique direction $[110]$, also perpendicular to the applied magnetic field (see figure 1c). At this field, the AFM and FM components of the KGM magnetic moment are found ≈ 1.5 and $2.4 \mu_B$ respectively from neutron and magnetization measurements.

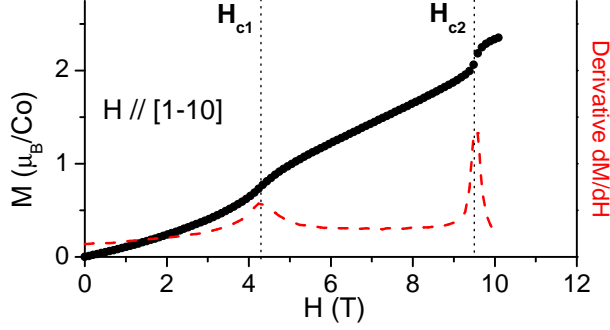


FIG. 4: Single-crystal magnetization and its derivative (red dashed line) measured as a function of the magnetic field oriented along the $[1-10]$ direction at 2 K

The scenario accounting for the field dependence of the magnetic ordering is thus the following: at zero-field, we assume that both the TRI and KGM moments are parallel to each other and along the 12 equivalent $\langle 112 \rangle$ directions. Increasing the field applied along $[1-10]$ selects the two $[11-2]$ and $[112]$ directions perpendicular to it, and thus the two associated \mathbf{k}_1 and \mathbf{k}_2 domains. \mathbf{H}_{c1} then marks an AFM to FM transition of the TRI magnetic moments that become aligned with the field. At \mathbf{H}_{c2} , a new magnetic order is stabilized with the AFM component on the KGM sites aligned along the $[110]$ direction. This orientation is compatible with the selection of two new domains, \mathbf{k}_3 and \mathbf{k}_4 , and implies a redefinition of the canted KGM and FM TRI planes.

TABLE I: Magnetic domain selection under a magnetic field applied along $[1-10]$: For the three field ranges given in the Table, the columns indicate the selected propagation vectors and the orientation of the antiferromagnetic component of the KGM and TRI magnetic moments. At $H=0$ T, the four magnetic domains are equipopulated and above \mathbf{H}_{c1} , the TRI moments are ferromagnetically aligned along the field.

$\mathbf{H}_{dom} < H < \mathbf{H}_{c1}$			$\mathbf{H}_{c1} < H < \mathbf{H}_{c2}$			$\mathbf{H}_{c2} < H$		
k	KGM	TRI	k	KGM	TRI	k	KGM	TRI
\mathbf{k}_1	$[11-2]$	$[11-2]$	\mathbf{k}_1	$[11-2]$	none	\mathbf{k}_3	$[110]$	none
\mathbf{k}_2	$[112]$	$[112]$	\mathbf{k}_2	$[112]$	none	\mathbf{k}_4	$[110]$	none

B. Structural changes

Correlated to the complex magnetic behavior of GeCo_2O_4 , there is a remarkable variation of the extinction. It corresponds to a decrease of the intensity of strong Bragg reflections when the structural crystal quality is improved [5]. An irreversible decrease of the intensity is observed on the intense nuclear reflection $(-4, -4, 0)$ up to \mathbf{H}_{dom} (see figure 3c) which shows that the struc-

tural quality is improved when the magnetic domains are selected. The intensity is then constant up to \mathbf{H}_{c2} where a very narrow peak of extra intensity is visible, indicating a transient crystal deterioration at the transition toward the new magnetic structure.

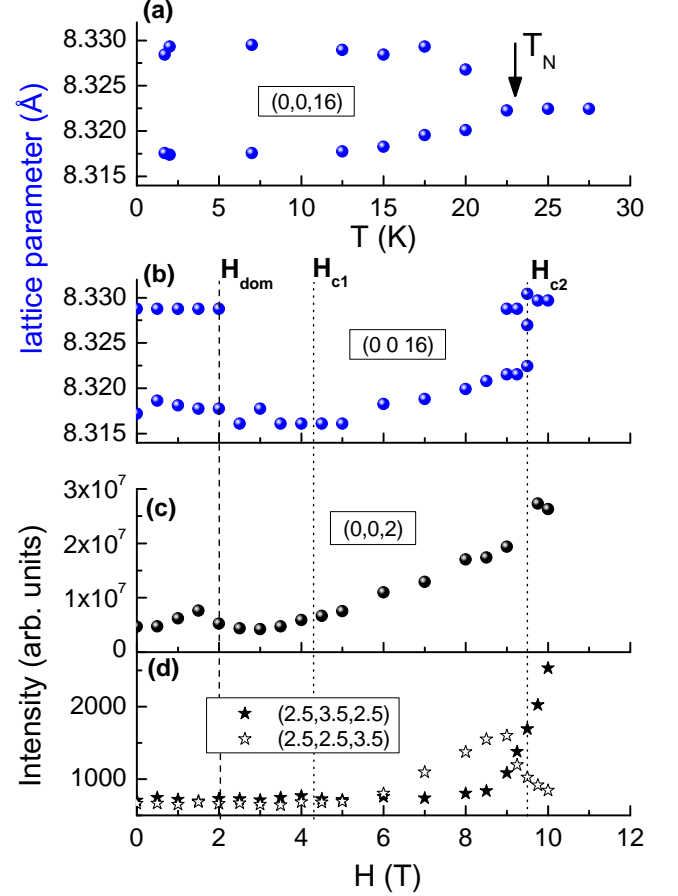


FIG. 5: Single-crystal X-ray diffraction: temperature dependence in zero field of the lattice parameter determined from the $(0, 0, 16)$ reflection (a). Field dependence at 2 K under a magnetic field along the $[1-10]$ direction of the lattice parameter determined from the $(0, 0, 16)$ reflection (b), of the intensity of the $(0, 0, 2)$ forbidden reflection (c), and of the intensities of the $(5/2, 5/2, 7/2)$ and $(5/2, 7/2, 5/2)$ Bragg reflections. This highlights a structural contribution associated to the \mathbf{k}_2 and \mathbf{k}_4 AFM domains respectively (d). The \mathbf{H}_{dom} , \mathbf{H}_{c1} and \mathbf{H}_{c2} characteristic fields are indicated by vertical lines.

These magnetostructural effects were further investigated by single-crystal X-ray diffraction on ID06. Back to the temperature dependence in zero field, the $(0, 0, 16)$ structural reflection splits into two peaks below T_N (see figure 5a). This agrees with a main cubic-to-tetragonal structural distortion implying a 0.12 % elongation of one of the cubic axes [4], hence yielding three tetragonal domains (see figure 6). It should be noted however that

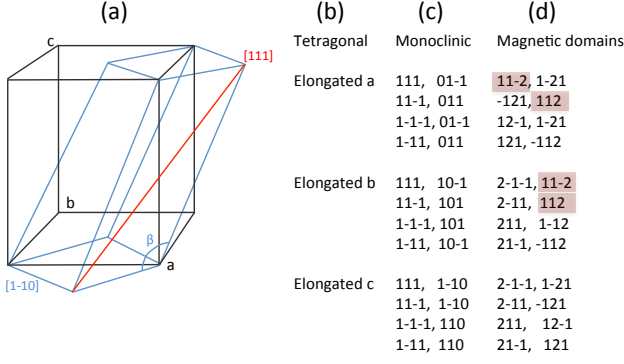


FIG. 6: Structural and magnetostructural domains. From left to right: (a) example of monoclinic cell (in blue) derived from the tetrahedrally distorted cubic cell (black) with the elongated c axis. The monoclinic distortion is achieved when the β angle deviates from 125.264° ; (b) 3 tetragonal domains characterized by their elongated axis; (c) 12 monoclinic domains characterized by the trigonal axis of the cubic cell and the monoclinic 2-fold axis; (d) associated 24 magnetic domains displaying the magnetization direction closest to the plane perpendicular to the tetragonal axis. The domains selected by a magnetic field applied along the $[1-10]$ direction are highlighted by red boxes.

a $(1/2, 1/2, 1/2)$ propagation vector for the magnetic structure is not compatible with the tetragonal symmetry in a single- k picture. A tetragonal distortion would imply 4 propagation vectors and a non-collinear magnetic structure. This is hardly compatible with the field-induced magnetic domain selection that we observe and that we can explain straightforwardly in a single- k magnetic structure. Similarly to CoO [9, 10, 23], we therefore suggest that the single- k structure is enabled by an additional small trigonal distortion superimposing the main tetragonal one. This should lead to a monoclinic space group, that has still to be evidenced. It is characterized by a unique 2-fold axis along the $\langle 110 \rangle$ direction perpendicular to the selected cubic trigonal $\langle 111 \rangle$ direction and to the tetragonal axis. In this case, each tetragonal domain is further split into three monoclinic domains, yielding 12 structural domains correlated to the magnetic ones. In particular, the trigonal cubic axis characterizing the distortion gives the direction of the magnetic propagation vector (see figure 6).

Under a magnetic field along $[1-10]$, the two $(0, 0, 16)$ peaks are still visible up to $H_{\text{dom}} = 2$ T, but only one peak remains above H_{dom} associated to the smaller lattice parameter (see figure 5b). It means that the field selects two tetragonal domains out of three, with an a or b elongated axis. It has been shown that the magnetic moment of Co^{2+} in a strain-induced tetragonally distorted CoO with an elongated tetragonal axis should lie perpendicular to this axis [28]. Our single-crystal neutron diffraction results indicate that $H \parallel [1-10]$ selects the magnetostructural domains with the $[112]$ and $[11-2]$

magnetic moments directions. These are closer to the (100) and (010) planes than to the (001) one, hence compatible with the a and b elongated axis, as observed.

From H_{c1} to H_{c2} , the position of the remaining peak progressively changes signaling an increase of the c lattice parameter. Above H_{c2} , a unique peak finally appears abruptly shifted at a value corresponding to a larger c lattice parameter. In addition to the lattice parameter variation, other structural changes start to occur for $H > H_{c1}$. The $(0, 0, 2)$ structural reflection, forbidden by the $4_1/d$ symmetry element of the $\text{Fd-}3m$ space group, rises in intensity from H_{c1} to H_{c2} where it presents a marked step, as observed both with neutron and X-ray diffraction (see figures 3d and 5c) [29]. Above H_{c1} , a structural contribution is also measured by X-ray diffraction on the Bragg peaks indexed by the propagation vectors of the type $(1/2, 1/2, 1/2)$ (see figure 5d). This indicates a doubling of the structural unit cell along the 3 crystallographic axes in connection with the magnetic domains.

III. DISCUSSION

These results provide a strong indication that the field-induced evolution of the magnetic structure of GeCo_2O_4 is not merely due to an energy balance between the Zeeman term, the magnetic exchange interactions and the single ion magnetocrystalline anisotropy. The key ingredient is actually the magnetostructural coupling. The TRI and KGM sites, that were coupled in zero-field through the structural distortion at T_N , get decoupled above H_{c1} when the field strength is enough to polarize the TRI planes. This renders ineffective the zero-field structural distortion in reducing the magnetic frustration and lowering the energy of the system. It thus triggers new structural changes evidenced by the rise of the $(0, 0, 2)$ and $(1/2, 1/2, 1/2)$ type of structural reflections and the increase of the c lattice parameter. These magnetoelastic effects ultimately lead at H_{c2} to an abrupt structural change and to a novel magnetic configuration. The latter consists in a stacking of FM planes of KGM moments exhibiting a ferromagnetic and an antiferromagnetic components, both perpendicular to the $\langle 111 \rangle$ directions. The AFM component is now orientated along the $[110]$ direction, which implies the magnetic domain switching from \mathbf{k}_1 and \mathbf{k}_2 to \mathbf{k}_3 and \mathbf{k}_4 at H_{c2} , and a change in the KGM and TRI sites distribution.

This remarkable spin reorientation can be ascribed to a change of the magnetocrystalline anisotropy of the Co^{2+} ions induced by the structural deformation acting on the Crystal Field parameters. The exact nature of the structural changes occurring at H_{c2} cannot be unambiguously established though. From an analogy with the Cr spinels, the first possibility is that this is a transition towards a new structure of cubic symmetry with a lattice parameter enlarged with respect to the paramagnetic state. The second option rather implies a change of the selected

structural domains, triggered by the magnetism. The weakening of the structural distortion tilts the magnetic moments from the [112] and [11-2] directions to the (001) plane. The magnetic moments are then perpendicular to the c -axis thus favoring the tetragonal structural domain with the elongated c -axis instead of those with elongated a and b axes selected for $\mathbf{H}_{\text{dom}} < \mathbf{H} < \mathbf{H}_{\text{c2}}$. This is supported by the fact that the c lattice parameter above \mathbf{H}_{c2} is identical to the one of the zero-field domain that disappears above \mathbf{H}_{dom} . Finally, complementary studies are crucially needed, first to confirm the simple- k nature of the magnetic structure and the monoclinic distortion, and then to decide between the two above scenarios.

IV. CONCLUSION

In conclusion, the spinel compound GeCo_2O_4 exhibits common features to both Cr/V spinels and binary ox-

ides like CoO , in spite of different interaction schemes or different topology of the lattice. Our neutron and X-ray single-crystal study has shown that unconventional behaviors are generated by the strong interplay between the structural and frustrated magnetic degrees of freedom under the influence of an external magnetic field. The high field transition is particularly rich, involving deep structural changes and a reshuffling of the inhomogeneous magnetization distribution, associated to a unique field-induced change of magnetocrystalline anisotropy.

We thank J. Debray for the single-crystal orientation and polishing for the X-ray experiment, E. Lhotel, R. Ballou and J. Robert for fruitful discussions, and L. Chaix, S. Diaz and A. deMuer for their help during the single-crystal neutron diffraction experiments.

-
- [1] S.-H. Lee, C. Broholm, T. H. Kim, W. Ratcliff, S.-W. Cheong, Phys. Rev. Lett. **84**, 3718 (2000).
 - [2] H. Ueda, H. A. Katori, H. Mitamura, T. Goto, H. Takagi, Phys. Rev. Lett. **94**, 047202, (2005).
 - [3] H. Ueda, H. Mitamura, T. Goto, Y. Ueda, Phys. Rev. B **73**, 094415 (2006).
 - [4] M. Matsuda, H. Ueda, A. Kikkawa, Y. Tanaka, K. Katsumata, Y. Narumi, T. Inami, Y. Ueda, S.-H. Lee, Nature Physics **3**, 397 (2007).
 - [5] M. Matsuda, K. Ohoyama, S. Yoshii, H. Nojiri, P. Frings, F. Duc, B. Vignolle, G. L. J. A. Rikken, L.-P. Regnault, S.-H. Lee, H. Ueda, Y. Ueda, Phys. Rev. Lett. **104**, 047201 (2010).
 - [6] E. D. Mun, G.-W. Chern, V. Pardo, F. Rivadulla, R. Sinclair, H. D. Zhou, V. S. Zapf, and C. D. Batista, Phys. Rev. Lett. **112**, 017207 (2014).
 - [7] K. Penc, N. Shannon, H. Shiba, Phys. Rev. Lett. **93**, 197203 (2004).
 - [8] D. L. Bergman, R. Shindou, G. A. Fiete, L. Balents, Phys. Rev. Lett. **96** 097207 (2006).
 - [9] S. Diaz, S. deBrion, G. Chouteau, B. Canals, V. Simonet, P. Strobel, Phys. Rev. B **74**, 092404 (2006).
 - [10] M. Matsuda, T. Hoshi, H. Aruga Katori, M. Kosaka, H. Takagi, Journal of the Physical Society of Japan **80**, 034708 (2011).
 - [11] E. F. Bertaut, Vu Van Qui, R. Pauthenet, A. Murasik, J. Phys. **25**, 516 (1964).
 - [12] M. K. Crawford, R. L. Harlow, P. L. Lee, Y. Zhang, J. Hormadaly, R. Flippen, Q. Huang, J. W. Lynn, R. Stevens, B. F. Woodfield, J. Boerio-Goates, R. A. Fisher, Phys. Rev. B **68**, 220408 (2003).
 - [13] M. Matsuda, J.-H. Chung, S. Park, T. J. Sato, K. Matsuno, H. Aruga Katori, H. Takagi, K. Kakurai, K. Kamazawa, Y. Tsunoda, I. Kagomiya, C. L. Henley, S.-H. Lee, Europhysics Letters, **82**, 37006 (2008).
 - [14] T. Hoshi, H. Aruga Katori, M. Kosaka, H. Takagi, Journal of Magnetism and magnetic Materials, **310**, E448 (2007).
 - [15] P. T. Barton, M. C. Kemei, M. W. Gaultois, S. L. Moffitt, L. E. Darago, R. Seshadri, M. R. Suchomel, B. C. Melot, Phys. Rev. B **90**, 064105 (2014).
 - [16] F. Plumier C. R. Acad. single-crystal. Paris, **264**, 278 (1967).
 - [17] S. Diaz, S. deBrion, M. Holzapfel, G. Chouteau, P. Strobel, Physica B **346**, 146 (2004).
 - [18] S. Diaz, S. deBrion, G. Chouteau, P. Strobel, B. Canals, J. Rodriguez-Carjaval, H. Rakoto, J.-M. Broto, J. App. Phys. **97**, 10A512 (2005).
 - [19] H. Sasame, H. Yoshimoto, Y. Takahashi, T. Watanabe, K. Takase, Y. Takano, S. Hara, SI. Ikeda, J. Phys.: Conf. Series **92**, 012154 (2007).
 - [20] T. Watanabe, S. Hara, S.-I. Ikeda, K. Tomiyasu, Phys. Rev. B **84**, 020409(R) (2011).
 - [21] T. Yamasaki, S. Okubo, H. Ohta, T. Sakurai, S. Ikeda, H. Oshima, M. Takahashi, S. Hara, K. Tomiyasu, T. Watanabe, J. Phys.: Conf. Series **400**, 032119 (2013).
 - [22] K. Tomiyasu, A. Tominaga, S. Hara, H. Sato, T. Watanabe, S.-I. Ikeda, H. Hiraka, K. Iwasa, and K. Yamada, J. Phys.: Conf. Series **320** 012038 (2011).
 - [23] see Supplemental Material for experimental details and additional neutron scattering results and analysis.
 - [24] Our measurements are not sensitive to the 180° domains, which are thus ignored.
 - [25] P. J. Becker and P. Coppens, Acta Crystallogr. Sect. A **30**, 129 (1974).
 - [26] W. Jauch, M. Reehuis, H. J. Bleif, F. Kubanek, and P. Pattison, Phys. Rev. B **64**, 052102 (2001).
 - [27] D. Herrmann-Ronzaud, P. Burlet, and J. Rossat-Mignod, J. Phys. C: Solid State Phys. **11** 2123 (1978).
 - [28] S. I. Csiszar, M. W. Haverkort, Z. Hu, A. Tanaka, H. H. Hsieh, H.-J. Lin, C. T. Chen, T. Hibma, L. H. Tjeng, Phys. Rev. Lett. **95**, 187205 (2005)
 - [29] The (0, 0, 2) reflection measured in neutron diffraction has both a nuclear and a FM contribution.

Supplemental material for "Field driven magnetostructural transitions in GeCo_2O_4 "

V. EXPERIMENTAL DETAILS

Powder patterns were recorded on the D2B high-flux diffractometer of the Institut Laue Langevin (ILL) under a magnetic field up to 6 T on a pressed pellet of GeCo_2O_4 at the wavelength $\lambda=1.594$ Å. Single crystal neutron diffraction was done in zero field and under magnetic field on two diffractometers at the ILL. Single-crystal diffraction in zero magnetic field was obtained on the CEA-CRG D15 diffractometer operated in the 4-circle mode, with the sample mounted in a 2 K displax refrigerator, and with an incident wavelength of 1.173 Å. Measurements under magnetic field up to 12 T was performed on the CEA-CRG D23 two-axis diffractometer with a lifting arm detector and an incident wavelength of 1.280 Å. The single-crystal was mounted in the cryomagnet with the $[1-10]$ axis set vertical, parallel to the applied field. An additional diffraction experiment using polarized neutrons with spherical polarization analysis was performed on the single-crystal installed inside the CRYOPAD device on the CEA-CRG IN22 spectrometer at the ILL using a wavelength of 2.36 Å. This set-up allows measuring the three orthogonal components of the polarization vector of the neutron beam after scattering by the sample whatever the direction of the incident neutron beam polarization. It gives for a reflection (Q_h, Q_k, Q_l) a polarization matrix \overline{P}_{ij} , with $i,j=X,Y,Z$ ($X \parallel$ scattering vector, $Z \perp$ the scattering plane) [1, 2].

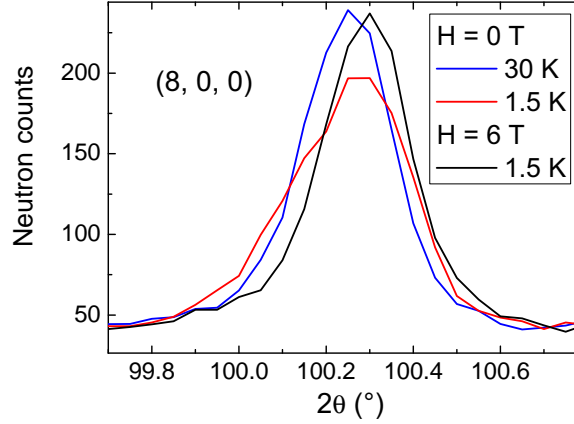


FIG. 7: Splitting of the $(0, 0, 8)$ nuclear reflection at T_N from powder neutron diffraction measurements on D2B.

High magnetic field X-ray single-crystal diffraction experiments were performed at the ID06 beamline of the European Synchrotron Radiation Facility using a monochromatic beam selected by a Si(111) double monochromator. Magnetic field was provided by a 10 T split-coil superconducting magnet [3]. A $2 \times 2 \times 1$ mm single-crystal was aligned with the $[110]$ and $[001]$ axes within the horizontal plane giving access to the (h, h, l) Bragg reflections. Magnetic field was applied along the $[-110]$ direction. The measurements were performed with two photons energy, either $E = 32$ keV ($\lambda = 0.3876$ Å) or $E = 7.67$ keV ($\lambda = 1.6165$ Å). The diffracted intensities were measured with a photodiode or a fast single-photon counting detector.

VI. COMPLEMENTARY NEUTRON SCATTERING RESULTS AND ANALYSIS

A. Powder neutron diffraction

In addition to single-crystal X-ray diffraction, we performed powder neutron diffraction under magnetic field to investigate the structural distortion. Our powder neutron measurements are in agreement with the proposed cubic-to-tetragonal main distortion occurring at T_N [4]. The large 2θ angle $(0, 0, 8)$ nuclear reflection splits into 2 below T_N with the lower angle reflection being twice smaller in intensity than the higher angle reflection (see figure 7). Under

a 6 T magnetic field, only the higher 2θ angle peak is still visible which corresponds to the selection of tetragonal domains with an elongated a or b axis.

B. Single-crystal neutron diffraction refinements

The nuclear and magnetic structures were refined from a large set of reflections using a program written with the IGOR software. The nuclear structure was first obtained at zero field and 10 K using the Bragg peak intensities collected on D15 by refining the scale factor, the Debye-Waller factor, the oxygen position parameter and the extinction [5]. The magnetic structure was obtained at $T=4.5$ K for zero field and for $H=5.5$, 9.4 and 12 T using the Bragg peak intensities collected on D23. The scale factor of the nuclear refinement was used and the direction and amplitude of the moments on the kagome and triangular sites, the population of S -domains, as well as the extinction parameter, were refined. The population of the k -domains was obtained by comparison of the intensities of equivalent reflections in the four domains. The results are summarized in the figure 8 and Table II. Note that there are some slight discrepancies between the calculated and observed integrated intensities in the nuclear and magnetic refinements, that were already pointed out in powder neutron diffraction works [6, 7]. They may be attributed to the structural changes occurring in the material that have not been taken into account in the analysis.

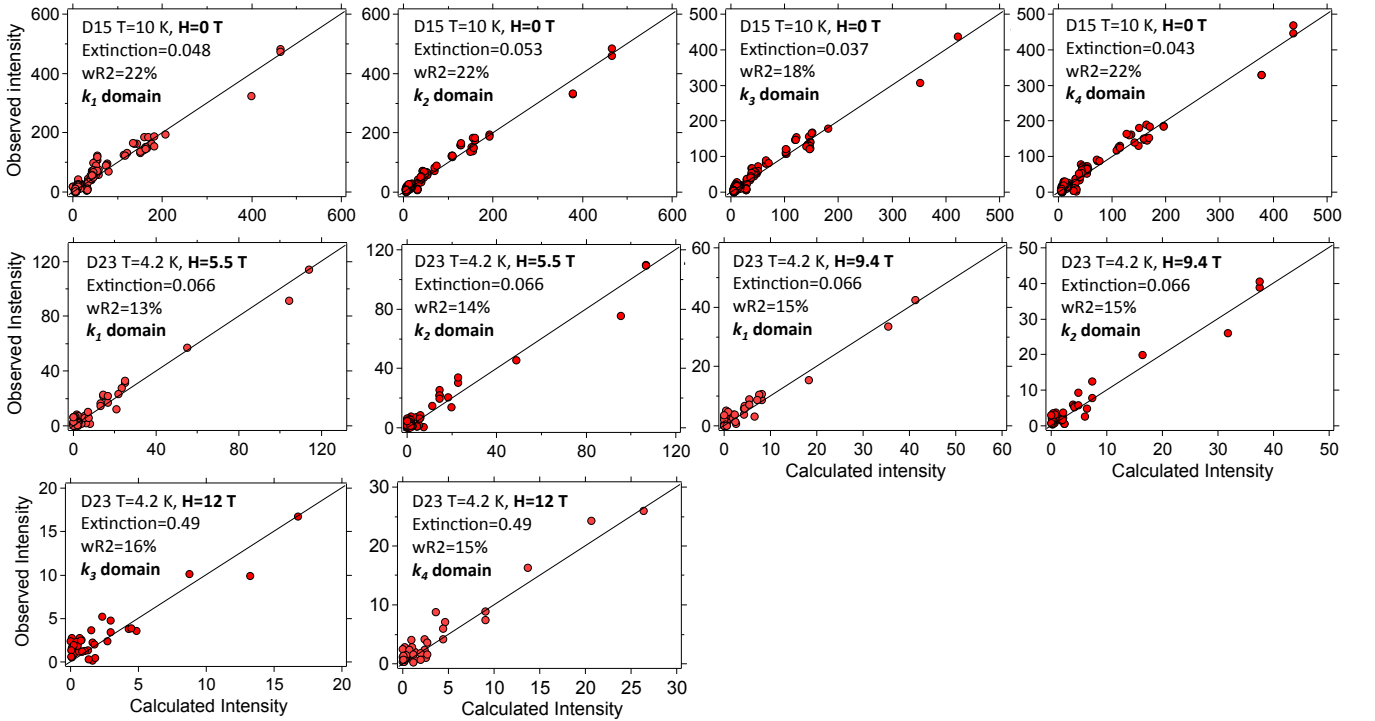


FIG. 8: Observed versus calculated intensity of the magnetic Bragg reflections refined at 0 T (a), at 5.5 T (b) and 9.4 T (c) and at 12 T (d).

Using polarized neutrons and spherical polarization analysis, we were able to get additional information about the respective orientation of the magnetic moments in zero-field. We have investigated 23 magnetic reflections of the k_1 domain at 1.5 K on IN22 using CRYOPAD. We have fitted the 9 components of the final normalized polarization of all the reflections, corrected from the background. The best fit is obtained for the TRI and KGM magnetic moments in the (111) plane, which are parallel to each other, with a population of the three S -domains equal to 26/40/34 %. Figure 9 shows the fit of the data, which gets worse when the angle between the two kinds of magnetic moments deviates from 0. Four points out of 207 are not well accounted for by the model. They correspond to the P_{YY} and P_{ZZ} components of the polarization matrix of the (0.5, 0.5, 2.5) and (1.5, 1.5, -0.5) reflections. The origin of this discrepancy is unclear at the moment but it could be related to the structural distortion.

	k -domain (%)	M_{KGM} (μ_B)	M_{TRI} (μ_B)	S -domain (%)
H=0 T, T=10 K, D15	k_1 0.255	3.3	2.2	0.34/0.28/0.38
	k_2 0.257	3.2	2.3	0.35/0.34/0.31
	k_3 0.234	3.2	2.2	0.35/0.34/0.31
	k_4 0.255	3.2	2.2	0.32/0.28/0.40
H=5.5 T, T=4.5 K, D23	k_1 0.510	(1.29, 1.29, -2.59)	0	0.97/0.015/0.015
	k_2 0.490	(1.27, 1.27, 2.53)	0	0.94/0.06/0.0
H=9.4 T, T=4.5 K, D23	k_1 0.510	(0.74, 0.74, -1.48)	0	0.99/0.0/0.01
	k_2 0.490	(0.71, 0.71, 1.43)	0	0.98/0.0/0.02
H=12 T, T=4.5 K, D23	k_3 0.605	(1.10, 1.10, 0)	0	1/0/0
	k_4 0.395	(1.09, 1.09, 0)	0	1/0/0

TABLE II: Results of the magnetic structure refinements at various magnetic fields. In the successive columns are reported the k -domains population, the magnetic moments on the kagome and triangular sites (only the amplitude at 0 T and the magnetic moment vectors under finite fields), and the population of the S -domains.

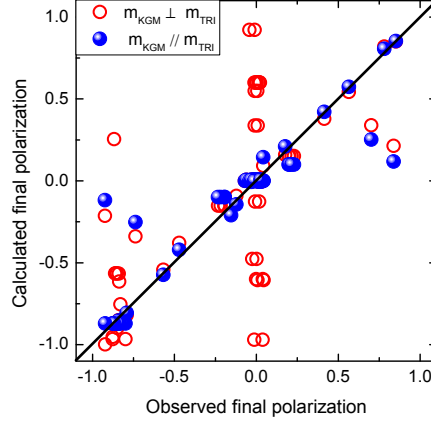


FIG. 9: Spherical polarization analysis at 1.5 K using CRYOPAD on IN22: calculated versus observed components of the final polarization for 23 magnetic Bragg peaks belonging to the k_1 domain. The magnetic moments on the sites TRI and KGM lie in the plane perpendicular to the (111) direction. They are either perpendicular to each other (red empty circles, $wR2=63.0\%$) or parallel (blue filled circles, $wR2=21.4\%$).

VII. COMPARISON WITH COO

A $(1/2, 1/2, 1/2)$ propagation vector for the magnetic structure is not compatible with the tetragonal symmetry in a single- k picture. A fundamental question is therefore whether the magnetic order is described by only one or several members of the star of the k -vector. A similar puzzling behavior was reported in CoO: this oxide was known to undergo a cubic-to-tetragonal structural transition at the temperature of the collinear magnetic ordering, itself described by an AFM stacking of ferromagnetic planes with a $(1/2, 1/2, 1/2)$ propagation vector and the magnetic moment along the $\langle 112 \rangle$ directions [8]. Symmetry arguments [9] were invoked showing that the tetragonal distortion actually implies a magnetic structure described by 4 propagation vectors, leading to a non-collinear magnetic structure. On the other hand, a single- k magnetic structure could be restored when an additional small trigonal distortion superimposes the main tetragonal one, leading to a monoclinic space group. In CoO, the evolution of the magnetic domains under applied stress allowed to discriminate between the two scenarios, in favor of a single- k structure [9]. A direct evidence of a small but finite trigonal lattice distortion was finally found [10], which agrees with the magnetic structure symmetry. Last, coexisting with the main magnetic order, a weak additional antiferromagnetic contribution with a tetragonal propagation vector $(0, 0, 1)$ was evidenced, consistent with the main structural distortion [11]. In analogy with CoO, we propose that GeCo_2O_4 enters a single- k magnetic order below T_N , compatible with a weak trigonal distortion added to the major tetragonal distortion of the paramagnetic cubic space group. This assumption is supported by the evolution of the magnetic domain population under magnetic field, as described in the main article. Also supporting this assumption is the orientation of the Co^{2+} magnetic moments that we determined along the same direction as in CoO. Last, a recent work has revealed an extremely weak additional $(1, 0, 0)$ magnetic reflection compatible with the

tetragonal symmetry [12] and coexisting with the main $(1/2, 1/2, 1/2)$ propagation vector.

-
- [1] F. Tasset, *Physica B* **156 & 157** 627 (1989).
 - [2] P.J. Brown, J.B. Forsyth and F. Tasset, *Proc. R. Soc. London A* **442** 147 (1993).
 - [3] L. Paolasini, C. Detlefs, C. Mazzoli, S. Wilkins, P. P. Deen, A. Bombardi, N. Kernavanois, F. De Bergevin, F. Yakhou, J. P. Valade et al., *Journal of Synchrotron Radiation* **14**, 1600 (2007).
 - [4] T. Hoshi, H. Aruga Katori, M. Kosaka, H. Takagi, *Journal of Magnetism and magnetic Materials* **310**, E448 (2007).
 - [5] P. J. Becker and P. Coppens, *Acta Crystallogr. Sect. A* **30**, 129 (1974).
 - [6] M. Matsuda, T. Hoshi, H. Aruga Katori, M. Kosaka, H. Takagi, *Journal of the Physical Society of Japan* **80**, 034708 (2011).
 - [7] S. Diaz, S. deBrion, G. Chouteau, B. Canals, V. Simonet, P. Strobel, *Phys. Rev. B* **74**, 092404 (2006).
 - [8] E. Ressouche, N. Kernavanois, L.-P. Regnault, J. Y. Henry, *Physica B* **385** (2006) 394.
 - [9] D. Herrmann-Ronzaud, P. Burlet, and J. Rossat-Mignod, *J. Phys. C: Solid State Phys.* **11** 2123 (1978).
 - [10] W. Jauch, M. Reehuis, H. J. Bleif, F. Kubanek, and P. Pattison, *Phys. Rev. B* **64**, 052102 (2001).
 - [11] K. Tomiyasu, T. Inami, and N. Ikeda, *Phys.Rev. B* **70** 184411 (2004).
 - [12] K. Tomiyasu, A. Tominaga, S. Hara, H. Sato, T. Watanabe, S.-I. Ikeda, H. Hiraka, K. Iwasa, and K. Yamada, *J. Phys.: Conf. Series* **320** 012038 (2011).